Cerium-Doped Yttrium Aluminum Garnet Hollow Shell Phosphors Synthesized via the Kirkendall Effect

Min Jeong Kim,[†,⊥] Jong Hoon Park,[‡] Keel Yong Lee,[§] Sangwook Lee,[∥] Gill-Sang Han,[†] Hee Jo Song,[‡] Hyunjung Shin,[§] Tae Kyu Ahn,*[,§] and Hyun Suk Jung*[,†]

[†]School of Advanced Materials Science and Engineering, Sungkyunkwan University, 2066 Seobu-ro, Janan-gu, Suwon-si, Gyeongi-do 440-746, Korea

[‡]Department of Materials Science and Engineering, Seoul National University, Gwanak-ro, Gwanak-gu, Seoul 151-742, Korea

[§]Department of Energy Science, Sungkyunkwan University, 2066 Seobu-ro, Janan-gu, Suwon-si, Gyeongi-do 440-746, Korea

[∥]Department of Material Science and Engineering, University of California, Berkeley, California 94709, United States

S *Supporting Information*

ABSTRACT: We report, for the first time, the synthesis of the $Y_3Al_5O_{12}$:Ce^{3+} hollow phosphor particles with a uniform size distribution via the Kirkendall effect, characterized by using a combination of *in situ* X-ray diffraction and high-resolution transmission electron microscopy analyses as a function of calcination temperature. The formation of hollow $Y_3Al_5O_{12}$:Ce^{3+} particles was revealed to originate from the different diffusivities of atoms (Al and Y) in a diffusion couple, causing a supersaturation of lattice vacancies. The optical characterization using photoluminescence spectroscopy and scanning confocal microscopy clearly showed the evidence of

YAG (yttrium aluminum garnet) hollow shells with emission at 545 nm. Another advantage of this methodology is that the size of hollow shells can be tunable by changing the size of initial nanotemplates that are spherical aluminum hydroxide nanoparticles. In this study, we synthesized the hollow shell particles with average diameters of 140 and 600 nm as representatives to show the range of particle sizes. Because of the unique structural and optical properties, the $Y_3Al_5O_{12}$:Ce^{3+} hollow shells can be another alternative to luminescence materials such as quantum dots and organic dyes, which promote their utilization in various fields, including optoelectronic and nanobio devices.

KEYWORDS: luminescence, YAG, Kirkendall effect, hollow spheres, phosphor nanoparticles, monodisperse
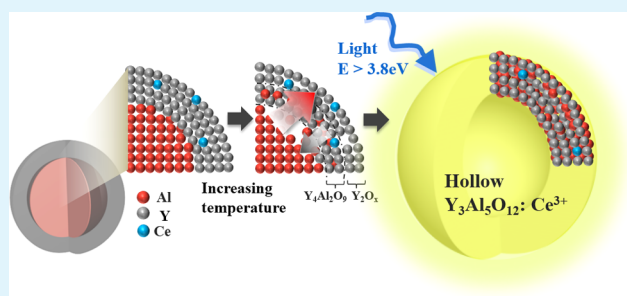
■ INTRODUCTION

Hollow nanomaterials[1−13] have attracted a great deal of interest because of their widespread applications in areas such as catalysis,[14] chromatography, drug carriers,[3,15−17] gas sensors,[11,12] and microcavity resonance due to their unique properties that include a low density, a high surface:volume ratio, a porous shell, a low coefficient of thermal expansion, and a low refractive index.[18,19] In particular, hollow luminescent nanoparticles, i.e., hollow shell phosphors, have been utilized in optoelectronic devices and multifunctional bioapplications, including display panels, photonic crystals, drug release, biosensors, and bioimage labeling. Moreover, the uniform size distribution of hollow shell phosphors is a prerequisite for the aforementioned applications, in terms of improvement in packing density and dispersion stability. Previously, preparations of $BaMgAl_{10}O_{17}$:Eu^{2+}, Gd_2O_3:Eu^{3+}, $EuPO_4 \cdot H_2O$, and $GdPO_4 \cdot H_2O$ hollow shell phosphors have been reported.[20−22] However, their particle size and uniformity could not be controlled. To control the particle size and uniformity of hollow shell phosphors, nanotemplate materials such as monodispersed SiO_2 and emulsions have been employed, and

consequently, quantum dots such as $CdSe$[15] and CdS[23] embedded hollow shells have been exploited. However, applications of these materials are limited by the toxicity of cadmium. Also, the template-mediated synthesis method requires post-treatment to remove the template, which causes contamination and damages the sample, which may weaken the luminescence.

Yttrium aluminum garnet ($Y_3Al_5O_{12}$, YAG), which is commonly used as a host material for phosphors, possesses a good chemical stability, a high quantum yield, a low toxicity, a low level of thermal expansion, and a tunable light emission wavelength.[24−26] Cerium-doped YAG (YAG:Ce^{3+}), emitting a yellow broad band spectrum, has been widely used as a white light-emitting diode combined with a blue light-emitting InGaN-based chip.[27] In addition, it is used for X-ray and γ-ray detectors (scintillators),[28−30] as well as biotechnology applications.[24,31] The luminescence characteristics of YAG:Ce^{3+}
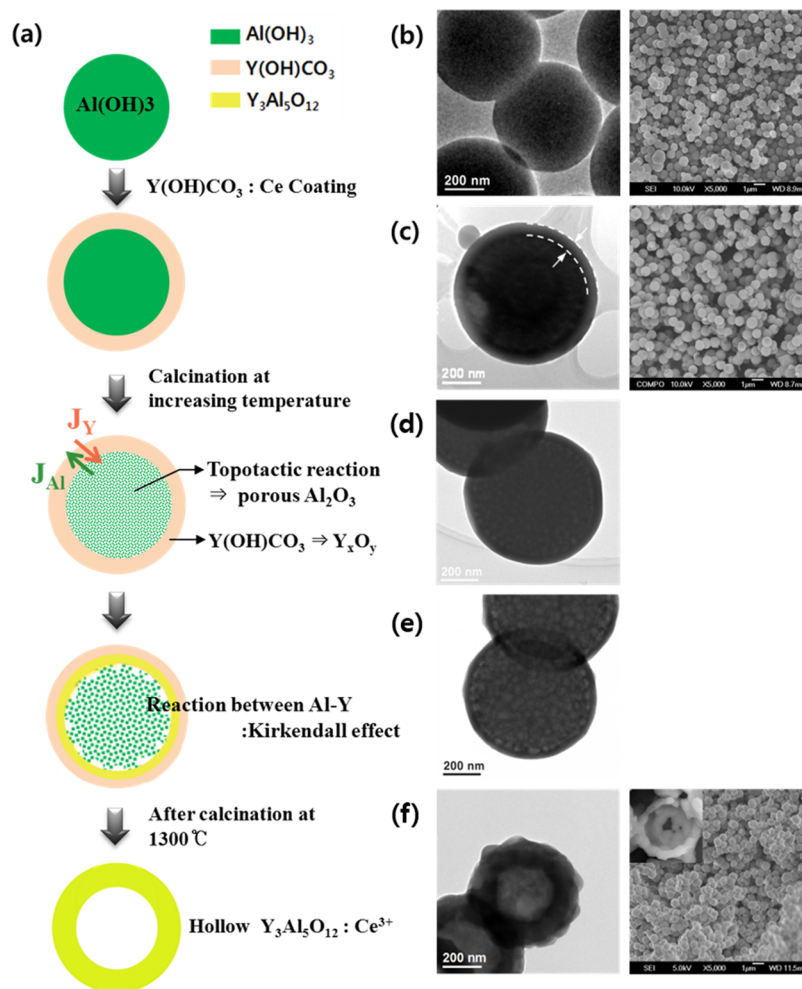
Figure 1. (a) Illustration of the sequential process for the synthesis of YAG:Ce^{3+} with TEM and SEM images of (b) $Al(OH)_3$ and (c) $Al(OH)_3$/$Y(OH)CO_3$ core−shell particles calcined at (d) 300, (e) 750, and (f) 1300 °C. The inset in panel f shows a sectional SEM image of a particle.

are affected by the morphology, crystallinity, and defects of particles. Conventionally, YAG:Ce^{3+} is synthesized by solid state reaction requiring a high reaction temperature of >1600 °C and mechanical milling, consequently resulting in an irregular morphology and deterioration of luminescence.[32−34] Recently, several synthesis methods, including sol−gel,[35] spray pyrolysis,[36,37] a microwave-assisted method,[38] and a solvothermal process,[39] have been investigated. However, all these previously described methods have not perfectly solved the problems such as the irregular shape and agglomeration of particles.

In this report, we have synthesized for the first time YAG:Ce^{3+} hollow phosphors with a narrow size distribution using monodisperse aluminum hydroxide nanoparticle templates. To the best of our knowledge, the synthesis of YAG hollow shells with a uniform size distribution has not previously been reported. The mechanism for the synthesis of YAG hollow phosphors is rationalized in terms of the Kirkendall effect. The Kirkendall effect[17,40−42] can be observed during the reaction between two species possessing different diffusivities. Vacancy diffusion compensates for the inequality of the material flow, leading to the formation of Kirkendall voids close to the interface between the core and shell. When the diffusion rate of core material is substantially faster than that of the shell material, the reaction yields a hollow shell structure as a result of the vacancy nucleation and growth inside the particles. To

establish the Kirkendall reaction condition, we coat the cerium-doped yttrium compound shell on the aluminum hydroxide and obtain YAG:Ce^{3+} through subsequent heat treatment. In addition, we have found that the size of the YAG hollow shells could be adjusted by changing the diameter of the aluminum hydroxide template.

■ RESULTS AND DISCUSSION

Figure 1 schematically illustrates the sequential process for synthesis of YAG:Ce^{3+} hollow spheres. Scanning electron microscopy (SEM) and transmission electron microscopy (TEM) micrographs clearly show the different steps of nanostructure fabrication. Monodisperse $Al(OH)_3$ nanoparticles with a diameter of 620 nm were synthesized using the forced hydrolysis process. TEM and SEM micrographs (Figure 1b) show the narrow size distribution of the aluminum hydroxide templates. Subsequently, Ce-doped yttrium basic hydroxide [$Y(OH)CO_3 \cdot H_2O$] was coated onto aluminum hydroxide core particles by controlling the nucleation and growth rate of $Y(OH)CO_3 \cdot H_2O$: Ce with the amount of added urea (see Figure S1 of the Supporting Information). Figure 1 shows that the $Y(OH)CO_3 \cdot H_2O$:Ce nanolayer with a thickness of 74 nm was uniformly coated onto the aluminum hydroxide. The $Y(OH)CO_3 \cdot H_2O$:Ce@$Al(OH)_3$ particles were annealed at temperatures of >900 °C, which yielded YAG:Ce^{3+} hollow
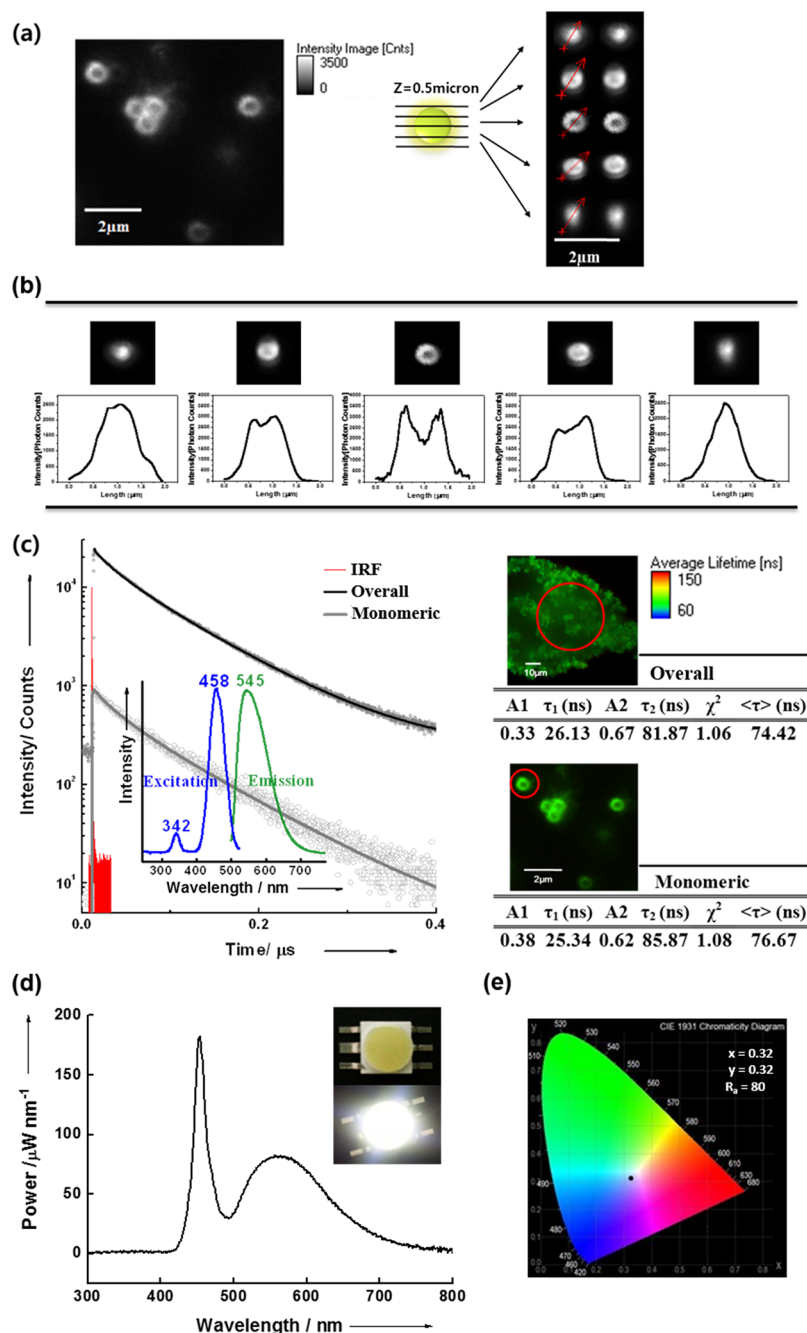
Figure 2. (a) Fluorescence confocal microscopy images and (b) photon intensity vs cross-sectional line scans of a YAG:Ce^{3+} single particle along the z-direction (y-axis, intensity in counts; x-axis, length in micrometers). (c) Fluorescence lifetime imaging microscopy (FLIM). The excitation wavelength was 485 nm at a power of <15 μW at a 1 MHz repetition rate. The emission of YAG:Ce^{3+} hollow shells was collected in a fast avalanche photodiode through a 500 nm cutoff filter to avoid any excitation light scattering. The time profile of the hollow particles was obtained for 20 ms for each pixel and was convoluted using the Symphotime program. The inset of panel c shows photoluminescence spectra (blue line, excitation; green line, emission). (d) EL spectra of the GaN LED with YAG:Ce^{3+}. The inset shows the photographs of the YAG:Ce^{3+}-based WLED. (e) International Commission on Illustration 1931 (CIE) coordinates of the YAG:Ce^{3+}-based LED (x = 0.321; y = 0.327).

shells. SEM images for YAG nanoparticles annealed at 1300 °C showed the hollow shell structure with a diameter of 597 ± 18 nm (see Figure S5 of the Supporting Information).

Each synthesized YAG:Ce^{3+} nanoparticle was characterized using a homemade confocal fluorescence lifetime imaging microscope as shown in Figure 2. High-resolution optical phosphor images (diameter of ∼600 nm) clearly showed that the YAG:Ce^{3+} nanoparticles possess a hollow shell morphology (Figure 2a). Along with the z-direction, a series of sequential

sectional confocal fluorescence images of YAG:Ce^{3+} at every 0.5 μm reveal the hollow shell morphology (Figure 2b). As shown in the excitation and emission spectra in the inset of Figure 2c, the YAG:Ce^{3+} hollow shell exhibited an excitation peak at 458 nm and an emission peak at 545 nm, which is consistent with commercial YAG:Ce^{3+}. To monitor the optical properties of each hollow, we measured fluorescence decays excited by a 485 nm laser pulse at room temperature. The YAG:Ce^{3+} hollow shell decay curve fitted a biexponential form

of $I = A_1 \exp(-t/\tau_1) + A_2 \exp(-t/\tau_2) + I_0$, where time constants τ_1 and τ_2 were in the range of 25−27 and 81−86 ns, respectively. The fast portion of the decay is likely due to the quenching of the cerium by the defects at the surface.[43] The resulting amplitude-weighted average fluorescence lifetime of YAG:Ce^{3+} was 74 ns. Considering that the lifetime for commercial YAG:Ce^{3+} powders with irregular shapes was ∼70 ns,[30] the YAG:Ce^{3+} hollow shells exhibit unperturbed photophysical properties. In addition, the overall hollow shells have a lifetime (τ) of 74 ns that is similar to that of monomeric hollow shells (76 ns), indicating that the aggregation does not affect the emissive states of individual hollows (Figure 2c). Therefore, we conclude that the YAG:Ce^{3+} hollow shells retain the original optical characteristics of the commercial material. Figure 2d shows the electroluminescence (EL) emission spectra of the YAG:Ce^{3+}-based LED under forward-bias DC currents of 100 mA, at room temperature. The emission peak centered at 450 nm was due to the radiative recombination from an InGaN active layer on the chip. The YAG:Ce^{3+} absorbed this light and emitted a broad emission band centered at 545 nm. Figure 2e shows the measured CIE chromaticity coordinated by the fabricated YAG:Ce^{3+}-based LED that is located in the white region ($x = 0.321$; $y = 0.327$; $R_a = 80$).

To provide some understanding of the mechanism of formation of YAG:Ce^{3+} hollow shells, we performed HRTEM analysis of YAG:Ce^{3+} particles as a function of annealing temperature as presented in Figure 3a. In the elemental mapping image of Y(OH)CO$_3$·H$_2$O:Ce@Al(OH)$_3$ particles (Figure 3b), the radius for the distribution of Y atoms was larger than that for the distribution of Al atoms, which indicated that the Y(OH)CO$_3$·H$_2$O layer covered the surface of the Al(OH)$_3$. The distribution of Ce atoms whose radius of distribution was approximately the same as that of Y indicates that Ce atoms were homogeneously doped into the Y(OH)CO$_3$·H$_2$O layer.

At an initial calcination temperature of 750 °C, thermal topotactic decomposition[44−46] of Al(OH)$_3$ produced highly nanoporous aluminum oxide core particles (Figure 1e). When the reaction temperature was increased to 900 °C, voids were also observed in the Y-based shell (Figure 3a) because yttrium basic carbonate was converted to yttrium oxide after decarbonation and dehydration of the particles (Figure S3 of the Supporting Information). In this step, some of the Al atoms reacted with Y atoms at the interface, leading to the formation of Al and Y compounds such as an Y$_4$Al$_2$O$_9$ phase. This Y-rich Y$_4$Al$_2$O$_9$ phase indicates that Al atoms diffused out to the core−shell interface (Figure 3d). When the reaction was conducted at 1000 °C, the YAlO$_3$ and Y$_3$Al$_5$O$_{12}$ (YAG) phases contained more Al atoms than the previously observed Y$_4$Al$_2$O$_9$ phase. As shown in the TEM image (Figure 3a), voids in the shell were eliminated, and the Al and Y compound shell became denser. It is noteworthy that the radius for distribution was identical for Al atoms and Y atoms in the elemental mapping (Figure 3b) at such high temperatures. These results imply that Al atoms fully diffuse out to the surface of the shell. Complete formation of the hollow particle was found at 1200 °C. This result can be rationalized as a consequence of the redistribution and coalescing of voids during the diffusion process, finally leading to formation of the hollow shell. Formation of a pure YAG phase was achieved at 1300 °C (Figure 3d). During the calcination process, the average radius of the hollow shell shrank to approximately 590 nm, corresponding to 80% of the initial diameter of the core−shell particle.
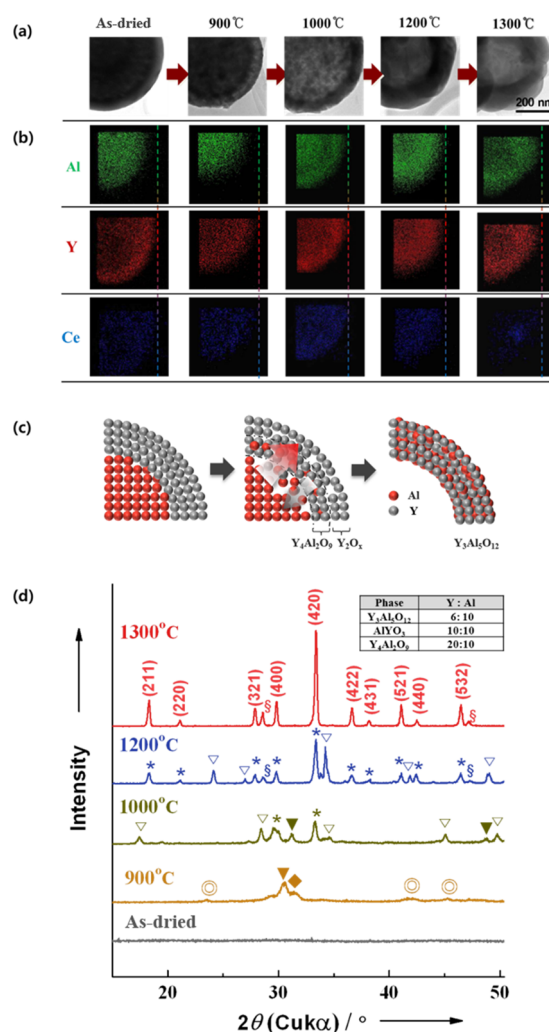

Figure 3. (a) HRTEM images of the Al(OH)$_3$/Y(OH)CO$_3$ core−shell particle with an increasing calcination temperature. (b) Distribution of aluminum, yttrium, and cerium determined by elemental mapping with EDX/TEM at each temperature. (c) Illustration of the diffusion process. (d) XRD patterns at different calcination temperatures: (*) Y$_3$Al$_5$O$_{12}$, (▼) Y$_4$Al$_2$O$_9$, (▽) AlYO$_3$, (§) CeO$_2$, (◆) Y$_2$O$_3$, and (◎) YO$_{1.401}$.

During formation of the YAG hollow shell, Al atoms diffused outward to the Y-based shell, indicating that the rate of diffusion of Al atoms was faster than that of Y atoms. There are several indications of the faster diffusion rate of Al atoms. First, formation of the Y-rich phase (Y$_4$Al$_2$O$_9$) was observed at a low calcination temperature (900 °C). Further, an annealing process over 1000 °C induced formation of YAlO and Y$_3$Al$_5$O$_{12}$ containing an Al atomic ratio higher than that of Y$_4$Al$_2$O$_9$ (Figure 3d). Second, as shown in Figure 4a, the ratio of shell thickness to particle radius increased with calcination temperature, implying that the interface between the core and shell moved inward; i.e., outward diffusion of Al atoms was dominant. Third, we did not observe any cracks in the YAG hollow shells. If inward diffusion of Y atoms had a rate faster than that of outward diffusion of Al, it left voids in the shell and consequently induced the formation of cracks in the shell. According to Wang et al.,[47] the formation of a hollow shell with cracks in the shell is dependent on the relative diffusion rate for atoms in the core and shell matter (Figure 4b[47]).
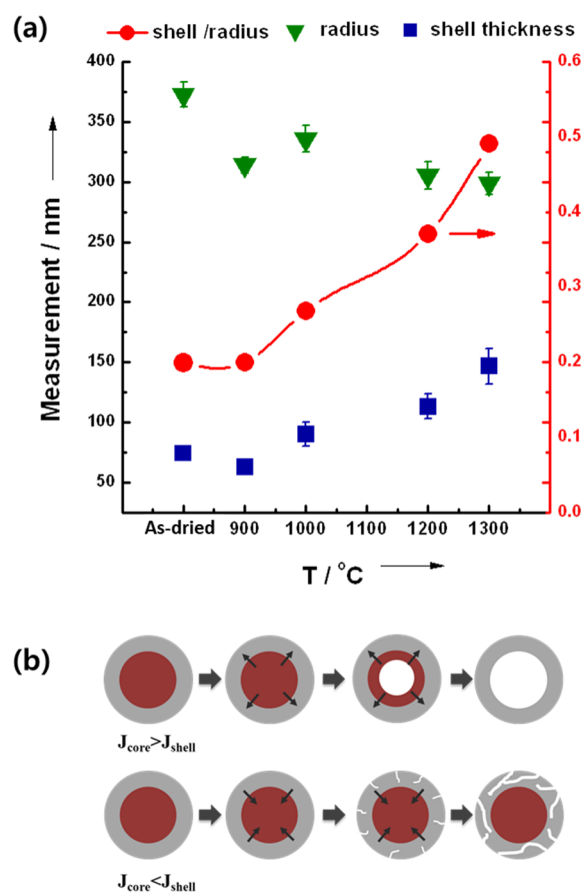
(a)

(b)

Figure 4. (a) TEM monitoring of the shell thickness per particle radius to analyze the movement behavior at the interface between $Al(OH)_3$ and $Y(OH)CO_3$. (b) Illustration of the Kirkendall effect depending on the relative diffusion rate.

Formation of the YAG hollow shell can be explained in terms of the Kirkendall effect. A typical characteristic for the Kirkendall effect is voids mostly observed at the interface between the core and shell.[48] In our results, voids generated by outward diffusion of Al atoms were apparent in the interface as shown in Figure 1e. The number of these voids increased with further calcination, which consequently led to the formation of a hollow shell structure. In other multicomponent ceramic systems, including $ZnAl_2O_4$, $MgAl_2O_4$, Cu_2O, SiO_2, and $CoSe_2$, the formation of hollow shells has similarly been explained in terms of the Kirkendall effect.[42]

We also fabricated smaller hollow $YAG:Ce^{3+}$ particles with an average diameter 147 ± 11 nm using $Al(OH)_3$ with a diameter of 176 ± 8 nm as the core particle. These data demonstrate that the size of the hollow shell YAG phosphor can be tuned by changing the $Al(OH)_3$ template particle size. Figure 5a exhibits the uniform size distribution of the hollow shell YAG phosphors. XRD data (Figure 5b) also show that the pure YAG phase can be obtained at 1100 °C, which is 200 °C lower than that for the 590 nm YAG hollow shell. This result is ascribed to the higher reactivity of smaller particles with a higher surface area.

CONCLUSIONS

In summary, we have for the first time fabricated $YAG:Ce^{3+}$ hollow shell phosphors with a uniform size distribution. In this process, yttrium basic carbonate-coated spherical aluminum

(a)

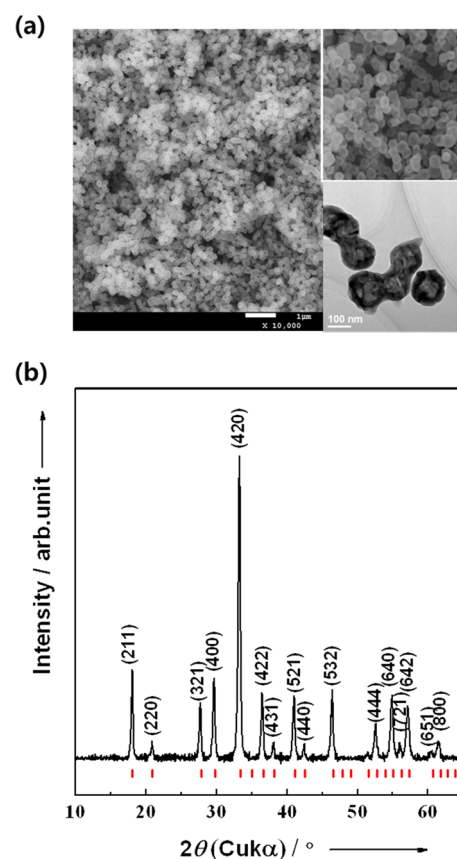**(b)**

Figure 5. $YAG:Ce^{3+}$ particles (147 nm): (a) SEM image and (b) XRD pattern. The inset of panel a is a TEM image of the particles.

hydroxide nanoparticles were annealed to yield hollow shell phosphors. This mechanism for particle formation has been attributed to the Kirkendall effect. This process can control the hollow shell size by changing the size of the aluminum hydroxide template. We also observed a 74 ns fluorescence decay time for the YAG hollow shell by FLIM analysis, which is similar to that of commercial YAG phosphors. Our results demonstrate that the $YAG:Ce^{3+}$ hollow shell particles could be applicable to optoelectronic devices such as next-generation LEDs.

MATERIALS AND METHODS

Synthesis of Aluminum Hydroxide Particles. Aluminum nitrate nonahydrate (Sigma-Aldrich, ≥98% pure), aluminum sulfate octade-cahydrate (Sigma-Aldrich, ≥98% pure) [Al^{3+} concentration of 0.01 M, aluminum nitrate:aluminum sulfate molar ratios of 0.3 for 620 nm $Al(OH)_3$ and 0.15 for 176 nm $Al(OH)_3$], and 0.1 M urea (Sigma-Aldrich, 99.5% pure) were dissolved in deionized water. Spherical aluminum hydroxide particles were obtained after the mixture had been aged at 98 °C for 4 h without being stirred. The precipitate was separated by centrifugation (8000 rpm for 5 min) and washed several times with deionized water.

Synthesis of Cerium-Doped Yttrium Aluminum Garnet. Yttrium(III) nitrate (Sigma-Aldrich, 0.02 M, 99.8% pure), cerium(III) nitrate (Sigma-Aldrich, 0.001 M, 99% pure), and urea (Sigma-Aldrich, 0.3 M, 99.5% pure) were dissolved in deionized water. Prepared aluminum hydroxide core particles (0.03 M) were dispersed homogeneously in the mixed solution. Aluminum hydroxide−yttrium basic carbonate core−shell particles were obtained by aging the solution while it was being vigorously stirred (500 rpm) at 85 °C for 3 h. The precipitate was isolated by centrifugation (8000 rpm for 5 min) and washed with deionized water several times. The core−shell

particles were dried with a lyophilizer.[22] The resulting powders were calcined at 1300 °C with a heating rate of 5 °C/min for 4 h in an oxygen flow and for an additional 2 h under a reducing atmosphere (5% H_2 and 95% N_2). To observe the morphology corresponding to XRD data, powders were calcined at 800, 900, 1000, and 1200 °C under the same condition.

LED Chip Fabrication. LEDs were fabricated by using InGaN LEDs with a surface mount device (SMD) type and YAG:Ce^{3+} phosphors. The phosphor was blended well with a transparent silicone resin, and then the blended resin mixture was mounted on the LED chip. Fabrication for the phosphor-converted LEDs (pc-LEDs) was completed after the defoaming and curing process had been conducted.

Characterization. The morphology was characterized using a high-resolution transmission electron microscope (JEM-3000F) and a scanning electron microscope (JSM-7600F). To observe the phase evolution, *in situ* high-temperature XRD measurements were taken with a Rigaku D/MAX-2500 instrument with Cu Kα radiation at 40 kV and 200 mA. We recorded *in situ* XRD patterns every 100 °C with a heating rate of 5 °C/min in air. The photoluminescent (PL) excitation and emission spectra of all the phosphors in the UV−vis range were measured using a fluorescence spectrometer (LS55, PerkinElmer). The emission spectra and CIE coordinate of the LED chip were measured using a spectroradiometer (ILT950, International Light Technologies, Inc.). Fluorescence lifetimes were measured with a home-built scanning confocal microscopy system. The YAG:Ce^{3+} hollow shell sample was excited with a pulsed diode laser (LDH-P-C-485B, 485 nm, PicoQuant) at a wavelength of 485 nm with a repetition rate of 1 MHz. The sample was placed on a piezo scanner (P-733.2CD, Princeton Instruments). The laser beam was reflected by a dichroic filter (FF495-Di03, Semrock) that was focused on the sample by a 100×, 1.4 oil-immersion objective lens (Olympus). The resulting fluorescence after the light had passed through a long-pass filter (>500 nm, FF01-496, Semrock) was collected by the same objective lens and finally detected by a single-photon avalanche photodiode (PDM-SPAD, Micro Photon Devices). The instrument response function had a full width at half-maximum of 100 ps. The output of the single-photon avalanche photodiode was recorded and analyzed by a time-correlated single-photon counting module (Picoharp300, PicoQuant). Experimental decays were numerically fit with two exponentials, with resulting χ^2 values between 1.0 and 1.2. From these fitted exponential components, average lifetimes were calculated according to the equation

$$\langle \tau \rangle = \frac{\sum A_i \tau_i^2}{\sum A_i \tau_i}$$

were A_i represents the amplitude at time zero and τ_i is the lifetime of the *i*th component. Fluorescence lifetimes were obtained using the analysis software (Symphotime and FluoFit, PicoQuant).

ASSOCIATED CONTENT

ⓢ Supporting Information

SEM images of Al(OH)$_3$@Y(OH)CO$_3$:Ce with urea concentrations, photoluminescence spectra with different urea:yttrium ratios, HRTEM image of the Al(OH)$_3$/Y(OH)CO$_3$ core−shell particle calcined at 300 and 750 °C, TG/DTG curves of Al(OH)$_3$/Y(OH)CO$_3$ powders in air, decay curve of YAG:Ce^{3+} particles with a controlled size of 147 ± 11 nm, and FIM-SEM images of 147 and 600 nm YAG:Ce^{3+} particles. This material is available free of charge via the Internet at http://pubs.acs.org.

AUTHOR INFORMATION

Corresponding Authors

*E-mail: taeahn@skku.edu.
*E-mail: hsjung1@skku.edu.

Present Address

⊥M.J.K.: School of Chemical and Biological Engineering, Seoul National University, Seoul 151-747, Korea.

Notes

The authors declare no competing financial interest.

REFERENCES

(1) Wang, Z.; Wu, L.; Chen, M.; Zhou, S. *J. Am. Chem. Soc.* **2009**, *131*, 11276−11277.

(2) Chen, M.; Wu, L.; Zhou, S.; You, B. *Adv. Mater.* **2006**, *18*, 801−806.

(3) Lv, R.; Gai, S.; Dai, Y.; Niu, N.; He, F.; Yang, P. *ACS Appl. Mater. Interfaces* **2013**, *5*, 10806−10818.

(4) Chen, M.; Hu, L.; Xu, J.; Liao, M.; Wu, L.; Fang, X. *Small* **2011**, *7*, 2449−2453.

(5) Hu, L.; Chen, M.; Shan, W.; Zhan, T.; Liao, M.; Fang, X.; Hu, X.; Wu, L. *Adv. Mater.* **2012**, *24*, 5872−5877.

(6) Hu, J.; Chen, M.; Fang, X.; Wu, L. *Chem. Soc. Rev.* **2011**, *40*, 5472−5491.

(7) Yoon, K.; Yang, Y.; Lu, P.; Wan, D.; Peng, H.; Stamm Masias, K.; Fanson, P. T.; Campbell, C. T.; Xia, Y. *Angew. Chem.* **2012**, *124*, 9681−9684.

(8) Ke, C.; Su, T.; Chen, H.; Liu, H.; Chiang, W.; Chu, P.; Xia, Y.; Sung, H. *Angew. Chem.* **2011**, *123*, 8236−8239.

(9) Hu, M.; Furukawa, S.; Ohtani, R.; Sukegawa, H.; Nemoto, Y.; Reboul, J.; Kitagawa, S.; Yamauchi, Y. *Angew. Chem.* **2012**, *124*, 1008−1012.

(10) Wei, W.; Ma, G. H.; Hu, G.; Yu, D.; Mcleish, T.; Su, Z. G.; Shen, Z. Y. *J. Am. Chem. Soc.* **2008**, *130*, 15808−15810.

(11) Li, X.; Lou, T.; Sun, X.; Li, Y. *Inorg. Chem.* **2004**, *43*, 5442−5449.

(12) Wu, Z.; Yu, K.; Zhang, S.; Xie, Y. *J. Phys. Chem. C* **2008**, *112*, 11307−11313.

(13) Caruso, F.; Caruso, R. A.; Möhwald, H. *Science* **1998**, *282*, 1111−1114.

(14) Liang, H. P.; Zhang, H. M.; Hu, J. S.; Guo, Y. G.; Wan, L. J.; Bai, C. L. *Angew. Chem.* **2004**, *116*, 1566−1569.

(15) Hao, L.; Gong, X.; Xuan, S.; Zhang, H.; Gong, X.; Jiang, W.; Chen, Z. *Appl. Surf. Sci.* **2006**, *252*, 8724−8733.

(16) Piao, Y.; Kim, J.; Na, H. B.; Kim, D.; Baek, J. S.; Ko, M. K.; Lee, J. H.; Shokouhimehr, M.; Hyeon, T. *Nat. Mater.* **2008**, *7*, 242−247.

(17) An, K.; Hyeon, T. *Nano Today* **2009**, *4*, 359−373.

(18) Zhang, C.; Li, C.; Peng, C.; Chai, R.; Huang, S.; Yang, D.; Cheng, Z.; Lin, J. *Chem.—Eur. J.* **2010**, *16*, 5672−5680.

(19) Lou, X. W. D.; Archer, L. A.; Yang, Z. *Adv. Mater.* **2008**, *20*, 3987−4019.

(20) Jung, K. Y.; Lee, D. Y.; Kang, Y. C.; Park, H. D. *J. Lumin.* **2003**, *105*, 127−133.

(21) Liu, G.; Hong, G.; Wang, J.; Dong, X. *J. Alloys Compd.* **2007**, *432*, 200−204.

(22) Guan, M.; Tao, F.; Sun, J.; Xu, Z. *Langmuir* **2008**, *24*, 8280−8283.

(23) Wu, D.; Ge, X.; Zhang, Z.; Wang, M.; Zhang, S. *Langmuir* **2004**, *20*, 5192−5195.

(24) Dong, B.; Wang, J.; Sun, J.; Xu, S.; Bai, X.; Jiang, Z.; Xia, L.; Sun, L.; Song, H. *RSC Adv.* **2012**, *2*, 3897−3905.

(25) Pedrini, C.; Rogemond, F.; McClure, D. *J. Appl. Phys.* **1986**, *59*, 1196−1201.

(26) Tomiki, T.; Akamine, H.; Gushiken, M.; Kinjoh, Y.; Miyazato, M.; Miyazato, T.; Toyokawa, N.; Hiraoka, M.; Hirata, N.; Ganaha, Y.; Futemma, T. *J. Phys. Soc. Jpn.* **1991**, *60*, 2437−2445.

(27) Baur, J.; Schlotter, P.; Schneider, J. *Adv. Solid State Phys.* **1998**, *37*, 67−78.

(28) Touš, J.; Horváth, M.; Pína, L.; Blažek, K.; Sopko, B. *Nucl. Instrum. Methods Phys. Res., Sect. A* **2008**, *591*, 264−267.

(29) Moszynski, M.; Ludziejewski, T.; Wolski, D.; Klamra, W.; Norlin, L. *Nucl. Instrum. Methods Phys. Res., Sect. A* **1994**, *345*, 461−467.

(30) David, S.; Michail, C.; Roussou, M.; Nirgianaki, E.; Toutountzis, A.; Valais, I.; Fountos, G.; Liaparinos, P.; Kandarakis, I.; Panayiotakis, G. *IEEE Transactions of Nuclear Science* **2010**, *57*, 951−957.

(31) Kandarakis, I.; Cavouras, D.; Sianoudis, I.; Nikolopoulos, D.; Episkopakis, A.; Linardatos, D.; Margetis, D.; Nirgianaki, E.; Roussou, M.; Melissaropoulos, P.; Kalivas, N.; Kalatzis, I.; Kourkoutas, K.; Dimitropoulos, N.; Louizi, A.; Nomicos, C.; Panayiotakis, G. *Nucl. Instrum. Methods Phys. Res., Sect. A* **2005**, *538*, 615−630.

(32) Ikesue, A.; Kinoshita, T.; Kamata, K.; Yoshida, K. *J. Am. Ceram. Soc.* **1995**, *78*, 1033−1040.

(33) Kinsman, K. M.; McKittrick, J.; Sluzky, E.; Hesse, K. *J. Am. Ceram. Soc.* **1994**, *77*, 2866−2872.

(34) Ikesue, A.; Furusato, I.; Kamata, K. *J. Am. Ceram. Soc.* **1995**, *78*, 225−228.

(35) Veith, M.; Mathur, S.; Kareiva, A.; Jilavi, M.; Zimmer, M.; Huch, V. *J. Mater. Chem.* **1999**, *9*, 3069−3079.

(36) Lee, S. H.; Jung, D. S.; Han, J. M.; Young Koo, H.; Kang, Y. C. *J. Alloys Compd.* **2009**, *477*, 776−779.

(37) Zhou, Y. H.; Lin, J.; Yu, M.; Han, S. M.; Wang, S. B.; Zhang, H. J. *Mater. Res. Bull.* **2003**, *38*, 1289−1299.

(38) Bhaskar, A.; Chang, H.; Chang, T.; Cheng, S. *Mater. Lett.* **2012**, *78*, 124−126.

(39) Li, X.; Liu, H.; Wang, J.; Cui, H.; Han, F. *Mater. Res. Bull.* **2004**, *39*, 1923−1930.

(40) Yin, Y.; Rioux, R. M.; Erdonmez, C. K.; Hughes, S.; Somorjai, G. A.; Alivisatos, A. P. *Science* **2004**, *304*, 711−714.

(41) Tu, K. *Appl. Phys. Lett.* **2005**, *86*, 093111.

(42) Fan, H. J.; Gtt, M.; Erdonmez, C. K. *Small* **2007**, *3*, 1660−1671.

(43) Furman, J. D.; Gundiah, G.; Page, K.; Pizarro, N.; Cheetham, A. K. *Chem. Phys. Lett.* **2008**, *465*, 67−72.

(44) Lee, S.; Kim, J. Y.; Youn, S. H.; Park, M.; Hong, K. S.; Jung, H. S.; Lee, J.; Shin, H. *Langmuir* **2007**, *23*, 11907−11910.

(45) Jung, H. S.; Lee, J.; Nastasi, M.; Lee, S.; Kim, J.; Park, J.; Hong, K. S.; Shin, H. *Langmuir* **2005**, *21*, 10332−10335.

(46) Glasser, L. D.; Glasser, F.; Taylor, H. *Q. Rev., Chem. Soc.* **1962**, *16*, 343−360.

(47) Wang, Y.; Cai, L.; Xia, Y. *Adv. Mater.* **2005**, *17*, 473−477.

(48) Fan, H. J.; Knez, M.; Scholz, R.; Hesse, D.; Nielsch, K.; Zacharias, M. G.; Shin, H. *Nano Lett.* **2007**, *7*, 993−997.